Extracellular Zinc Ion Inhibits ClC-0 Chloride Channels by Facilitating Slow Gating

Tsung-Yu Chen

From the Department of Physiology, National Yang-Ming University, Taipei 11221, Taiwan

ABSTRACT Extracellular Zn^{2+} was found to reversibly inhibit the ClC-0 Cl^- channel. The apparent on and off rates of the inhibition were highly temperature sensitive, suggesting an effect of Zn^{2+} on the slow gating (or inactivation) of ClC-0. In the absence of Zn^{2+}, the rate of the slow-gating relaxation increased with temperature, with a Q_{10} of ~37. Extracellular Zn^{2+} facilitated the slow-gating process at all temperatures, but the Q_{10} did not change. Further analysis of the rate constants of the slow-gating process indicates that the effect of Zn^{2+} is mostly on the forward rate (the rate of inactivation) rather than the backward rate (the rate of recovery from inactivation) of the slow gating. When ClC-0 is bound with Zn^{2+}, the equilibrium constant of the slow-gating process is increased by ~30-fold, reflecting a 30-fold higher Zn^{2+} affinity in the inactivated channel than in the open-state channel. As examined through a wide range of membrane potentials, Zn^{2+} inhibits the opening of the slow gate with equal potency at all voltages, suggesting that a two-state model is inadequate to describe the slow-gating transition. Following a model originally proposed by Pusch and co-workers (Pusch, M., U. Ludewig, and T.J. Jentsch. 1997. *J. Gen. Physiol.* 109:105–116), the effect of Zn^{2+} on the activation curve of the slow gate can be well described by adding two constraints: (*a*) the dissociation constant for Zn^{2+} binding to the open channel is 30 μM, and (*b*) the difference in entropy between the open state and the transition state of the slow-gating process is increased by 27 J/mol/°K for the Zn^{2+}-bound channel. These results together indicate that extracellular Zn^{2+} inhibits ClC-0 by facilitating the slow-gating process.

KEY WORDS: ClC-0 • Zn^{2+} • slow gating • inactivation • temperature dependence

INTRODUCTION

ClC-0, the first cloned member of the ClC channel family, is a voltage-dependent chloride channel that is present abundantly in the *Torpedo* electric organ. The open–close transition of this channel is known to involve two different gating processes, both of which are voltage dependent (for review, see Miller and Richard, 1990; Pusch and Jentsch, 1994). In one, the channel opens, or activates, when membrane potential is depolarized, and closes, or deactivates, when membrane potential is hyperpolarized. This transition happens in a relatively fast time scale of milliseconds and is thought to be controlled by a "fast" gate (Miller, 1982; Hanke and Miller, 1983; Pusch et al., 1995; Chen and Miller, 1996). The other gating process, which resembles inactivation of other voltage-gated channels, operates in a time scale of tens of seconds. This "slow" gate opens when membrane potential hyperpolarizes and closes when membrane potential depolarizes (White and Miller, 1979; Pusch et al., 1997). Previous studies have suggested that there are two identical "protomers" in a channel, each of which probably contains a pore and an independent fast gate (Miller, 1982; Middleton et al., 1994, 1996; Ludewig et al., 1996). On the other hand, the inactivation (or the close–open transition of the slow gate) occurs at the same time for the two protochannels (Miller and White, 1984; Richard and Miller, 1990; Pusch et al., 1997).

The above two gating processes function in an interesting way in that they both show Cl^- as well as voltage dependence. The fast gate decreases its open probability upon reducing the extracellular Cl^- concentration (Pusch et al., 1995), suggesting that the permeant ion, Cl^-, may act as the gating charge for the channel opening (Pusch et al., 1995; Chen and Miller, 1996). The interaction of Cl^- with the slow gating is even more intriguing. It was found that Cl^- flux through the channel pore was coupled to a nonequilibrium gating among closed, open, and inactivated states of the channel (Richard and Miller, 1990). The underlying mechanism of this phenomenon is still unknown. The slow gating of ClC-0 is difficult to characterize in a quantitative manner at the single channel level because the gate operates at a very slow rate. Recently, by measuring macroscopic current relaxation from *Xenopus* oocytes expressing ClC-0, Pusch et al. (1997) discovered that the inactivation rate of ClC-0 was highly temperature dependent with a Q_{10} of ~40.

The high temperature dependence of the slow gating of ClC-0 suggests that the process may involve a very

Address correspondence to Dr. Tsung-Yu Chen, Department of Physiology, National Yang-Ming University, #155, Sec. 2, Li-Nung Street, Shih-Pai, Taipei 11221, Taiwan. Fax: 886-2-2826-4049; E-mail: tychen@ym.edu.tw

complex conformational change of the channel molecule (Pusch et al., 1997). The mechanism underlying this complex slow-gating transition, however, is not well understood. There have been so far only a few point mutants of the channel whose slow-gating processes are altered (Ludewig et al., 1996, 1997). The amino acid residues that have been identified, however, are scattered throughout the entire channel sequence, making a mechanistic interpretation of the mutation effect rather difficult. Another problem that hinders a better understanding of ClC-0 inactivation comes from the fact that there are few useful molecular probes that can interfere with this gating transition. Previously, Cd^{2+}, Ni^{2+}, and Zn^{2+} have been shown to interact with the permeation and the gating processes in a variety of ion channels (Backx et al., 1992; Karpen et al., 1993; Yellen et al., 1994; Gordon and Zagotta, 1995; Liu et al., 1997). Results from studying the interaction of these divalent cations with channel proteins provide insightful information to understand not only the functional but also the structural aspects of these channel molecules. The interesting issue here is whether these useful metal ions are able to interact with ClC-0.

The modulation of ClC-type Cl^- channels by divalent metal ions is not without precedence. Early investigations have revealed that Zn^{2+} inhibits the resting conductance of the frog skeletal muscle (Hutter and Warner, 1967; Stanfield, 1970; Bretag et al., 1984), the majority of which is contributed by a Cl^- conductance, most likely ClC-1. Recently, human and rat ClC-1 channels were expressed in *Xenopus* oocyte, mammalian, and insect cell lines, and the channels were found to be irreversibly blocked by Zn^{2+} and Cd^{2+} (Kürz et al., 1997; Rychkov et al., 1997). The underlying mechanisms for these inhibitions, however, were not understood. ClC-0 is similar to ClC-1 not only in the amino acid sequence, but also in gating properties (Jentsch et al., 1990; Steinmeyer et al., 1991). In the present study, I show that Zn^{2+} can also inhibit the ClC-0 channel. Unlike in the case of ClC-1, the inhibition of ClC-0 by Zn^{2+} is reversible. Detailed characterization of this inhibition indicates that the effect appears to be due to a facilitation of the slow gating. This observation thus provides an opportunity of using Zn^{2+} to explore the molecular mechanism of the slow-gating process of ClC-0.

MATERIALS AND METHODS

Molecular Biology and Channel Expression

All experiments were carried out in *Xenopus* oocytes expressing wild-type ClC-0 originally cloned from *Torpedo* electric organ (Jentsch et al., 1990). The modified version of the cDNA, pRM105, in which most of the 3′ and 5′ untranslated regions were deleted, was first linearized by restriction enzyme ScaI (New England Biolabs Inc., Beverly, MA). Capped cRNA was then transcribed in vitro using the T3 mMessage mMachine kit (Ambion Inc., Austin, TX). *Xenopus* oocytes were surgically removed and dissociated for 1 h in nominally calcium-free OR-2 solution (containing [mM]: 96 NaCl, 2 KCl, 2 $MgCl_2$, and 5 Na-HEPES, pH 7.6) containing 1 mg/ml of type II collagenase (GIBCO BRL, Gaithersburg, MD). Follicle-free stage V–VI oocytes were selected and injected with 50 nl synthetic mRNA in distilled water (0.01–0.2 mg/ml). Injected oocytes were maintained at 18°C (±3°C) in ND96 solution (containing [mM]: 96 NaCl, 2 KCl, 1.8 $CaCl_2$, 1 $MgCl_2$, and 5 Na-HEPES, pH 7.6, plus 0.2 mg/ml gentamicin) and, with daily change of the ND-96 maintaining solution, were usually able to survive for 7–10 d.

Electrical Recording and Data Analysis

Whole oocyte ClC-0 current was recorded with a two-electrode voltage clamp amplifier (725C; Warner Instruments, Hamden, CT) 1–4 d after mRNA injection. Microelectrodes were filled with 3 M KCl and had resistance of 0.2–1.0 MΩ. The current, filtered at 1 kHz by the built-in filter of the amplifier, was digitized at 2–5 kHz using Digidata 1200 data acquisition board and pClamp6 software (Axon Instruments, Foster City, CA). Expression of ClC-0 was checked with a voltage protocol similar to that shown in Fig. 2 *A*. This protocol elicited a characteristic current crossover in the voltage range from −150 to −80 mV in the injected oocytes (see Fig. 2 *B*), indicating a successful expression of ClC-0.

For a typical experiment, the recording room was set at the desired temperature. Oocytes were then brought out of the incubating chamber to equilibrate the temperature of incubating solution to the room temperature at least 30 min before recording. The bathing (external) solution for assaying the effect of Zn^{2+} was a low Ca^{2+}–ND96 solution containing (mM): 96 NaCl, 2 KCl, 0.3 $CaCl_2$, 1 $MgCl_2$, and 5 Na-HEPES, pH 7.6. $ZnCl_2$ (J.T. Baker, Inc., Phillipsburg, NJ) and chloride salts of other transition metals were dissolved in water as 100 mM stock solution and then added to the low Ca^{2+}–ND96 solution to obtain the indicated concentration.

To examine the kinetics of the slow-gating process, the slow gate was first opened with multiple short hyperpolarized pulses (−120 to −150 mV, 50–200 ms in duration) given at a frequency of 0.5–1 Hz. The membrane potential was then held at −30 mV, a value close to the equilibrium potential of Cl^-, and a 100-ms voltage pulse to +40 mV was given every 2–6 s to monitor the current relaxation. The frequency of the given +40-mV voltage pulses had no effect on the slow-gating relaxation rate.

To evaluate the effects of Zn^{2+} and other metal ions, the oocyte current was monitored with repetitive voltage pulses at a constant holding potential, usually −30 mV. The metal ions were applied only after the current reached a steady state. EGTA–ND96 solution was used as the control and wash solutions. Its composition was the same as that of the low Ca^{2+}–ND96 solution, except that an additional 1 mM $CaCl_2$ and 1 mM EGTA was added, with the pH adjusted to 7.6 after addition of the extra components. Since EGTA has a higher affinity for Zn^{2+} than for Ca^{2+}, the wash solution chelates any leftover Zn^{2+} (Yellen et al., 1994). The switch between EGTA–ND96 solution and low Ca^{2+}–ND96 solution causes little change in the current amplitude. For more precise measurements of the on and off rates of Zn^{2+} inhibition (see Fig. 3 *A*), the flow rate was at ~25 ml/min, whereas the volume of the recording chamber was ~1 ml. The time constant of the solution exchange was ~2 s, as judged from the time course of tetraethylammonium (TEA)[1] inhibition of a *Shaker* K^+ channel (see Fig. 3 *B*). It therefore took ~5–6 s to exchange the

[1]*Abbreviation used in this paper:* TEA, tetraethylammonium.

solution of the recording chamber to 99%. This delay was relatively small in comparison with the time constants of the slow gating of ClC-0 in most experiments. As the slow gating of ClC-0 and the Zn^{2+} inhibition were highly temperature dependent, all solutions used for recording were incubated at the desired temperature before use. The temperature of the perfusion solution was monitored by a small temperature-sensitive element (Warner Instruments). Typically, its variation was less than ±0.3°C throughout an experiment.

The ClC-0 current amplitude was usually measured near the end of the +40-mV voltage pulse when the opening of the fast gate is at steady state. Because the channel does not close completely even at very negative membrane potential (Chen and Miller, 1996; Ludewig et al., 1997), the nonspecific "leak" current was not subtracted in all experiments. The leak fraction, however, was estimated separately with two approaches. In one set of experiments, oocytes without mRNA injection were recorded in low Ca^{2+}–ND96 solution. Alternatively, oocytes expressing ClC-0 were recorded in 0 Cl^- solution (containing [mM]: 98 Na-Glutamate, 1.3 $MgSO_4$, and 5 Na-HEPES, pH 7.6), a condition in which the inward Cl^- flux is abolished. The measurements in both cases gave leak currents at +40 mV of ~0.1–0.2 μA, which were usually <2–3% of the maximal current in a typical oocyte used in this study. Little current difference between these two ways of leak measurements was discerned, indicating that the endogenous Cl^- current of the oocytes did not contribute much to the observed current.

Data analysis was conducted with software programs in pClamp6 (Axon Instruments) and Origin 4.0 (Microcal Software, Inc., Northampton, MA). Curve fittings were performed with an un-weighted least-squares method. Results are presented as mean ± SEM.

RESULTS

Sensitivity of ClC-0 to Various Divalent Metal Ions

Fig. 1 *A* shows the effects of several divalent metal ions on the steady state current of the oocyte. These metal ions have different potencies to inhibit the current. The comparison among various ions can usually be carried out on the same oocyte since the inhibition is reversible after the ion is washed out. In these experiments, Zn^{2+} had the strongest effect to inhibit ClC-0 with an apparent IC_{50} of ~1–3 μM (Fig. 1 *B*). Cd^{2+} and Ni^{2+} can also inhibit the current, but with a weaker effect. On the other hand, Co^{2+} and Mn^{2+} had almost no effect at concentrations up to 1–1.3 mM.

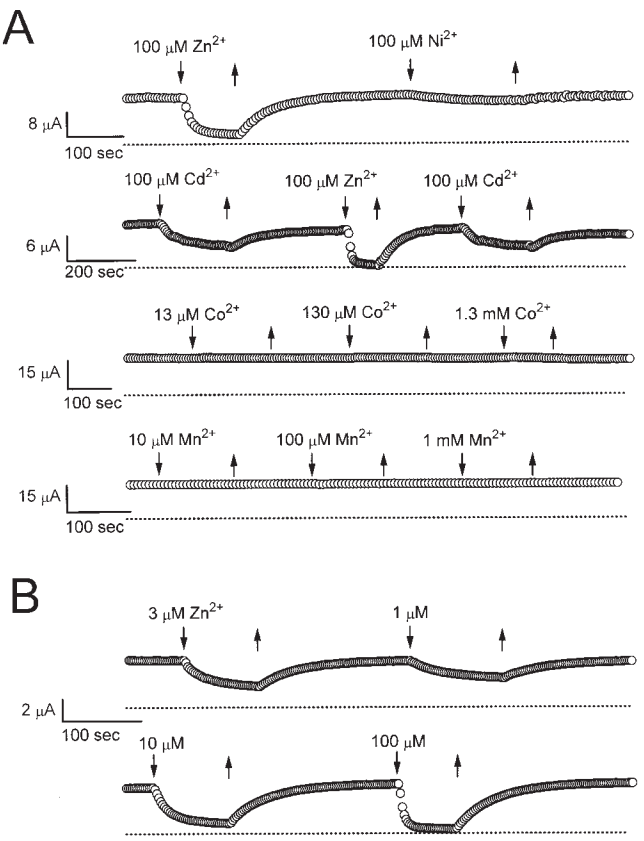

FIGURE 1. (*A*) Effects of various divalent metal ions on the steady state current of the ClC-0 Cl^- channel. The membrane potential of the oocyte was clamped at −30 or −40 mV. Each circle represents the current amplitude monitored by a 100-ms voltage pulse to +30 or +40 mV given every 5 or 6 s. Dotted lines show zero-current level. Solutions containing desired concentrations of various heavy metal ions were perfused in (*downward arrows*) and out (*upward arrows*), as indicated. (*B*) Concentration-dependent inhibition of the steady state current by Zn^{2+}. Holding potential was at −30 mV. Continuous recording at 27.4°C for more than 50 min.

Extracellular Zn^{2+} Has Little Effect on the Fast Gating of ClC-0

Although Zn^{2+} can reduce the steady state current of ClC-0 with relatively high affinity, its effect on the fast gate of the channel is only minimal. Fig. 2 *A* shows the voltage protocol similar to that used by Pusch et al. (1995) to examine the fast gating of ClC-0. The current families elicited by this voltage protocol in the absence or presence of Zn^{2+} were shown in Fig. 2 *B*. Application of 10 μM Zn^{2+} inhibits the current by about half at all voltages (Fig. 2 *B, left* and *middle*), indicating a voltage-independent inhibition. The current recovers completely after Zn^{2+} washout (Fig. 2 *B, right*).

The effect of Zn^{2+} on the fast gate of ClC-0 was evaluated in two ways: the steady state open probability (P_o) and the kinetics of the fast gate. To determine the P_o of the fast gate from Fig. 2 *B*, the tail current was extrapolated to the onset of period 4. Normalization of these extrapolated values to the maximal value (usually the one following the +80-mV test pulse) yielded the relative P_o's at the corresponding membrane potentials in period 3 (Pusch et al., 1995). Fig. 2 *C* shows that the steady state P_o–V curves in the presence and absence of Zn^{2+} are identical, indicating that Zn^{2+} has little effect on the fast gate. The effect of Zn^{2+} on the kinetics of the fast gate was evaluated by examining the fast-gating relaxation. The current deactivation in period 3 was fitted to a single-exponential function (Pusch et al., 1997; Ludewig et al., 1997) and the time constants at various voltages were plotted in Fig. 2 *D*. The effect of Zn^{2+} on

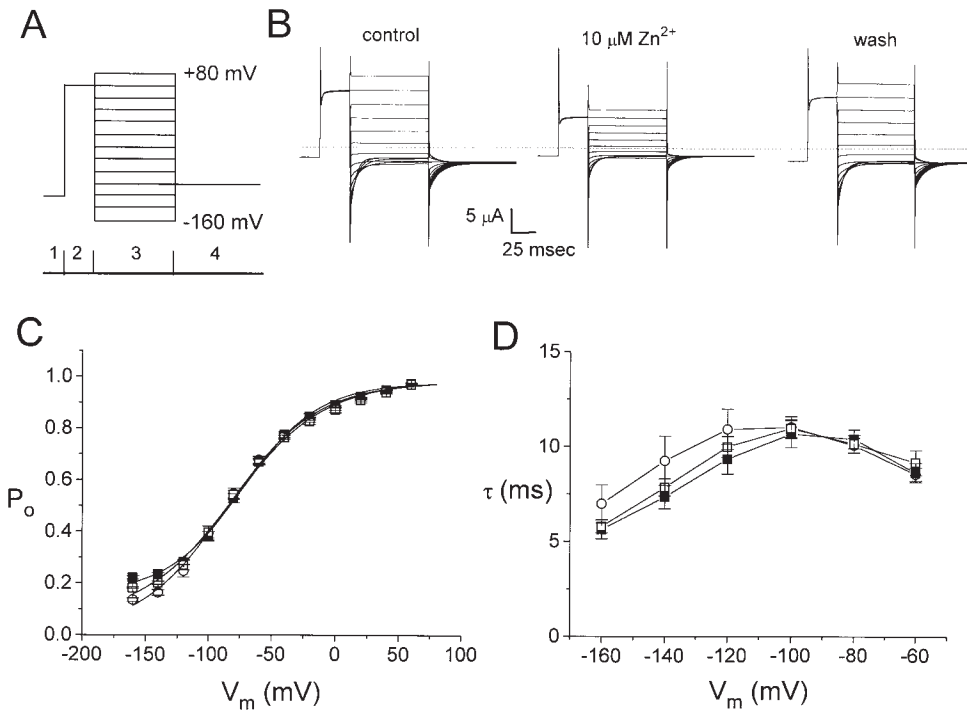

FIGURE 2. Extracellular Zn^{2+} has little effect on the fast gate of ClC-0. (*A*) Voltage protocol used to evaluate the fast gate of ClC-0. To focus on the fast gate, multiple short negative voltage pulses were applied to open the slow gate before the experiment. A −120-mV voltage step was first given to further ensure maximal activation of the slow gate (only partially shown in *1*). The fast gate was then examined with a voltage pulse to +60 mV (*2*), followed by different test voltages from −160 to +80 mV in 20-mV steps (*3*). The tail currents were measured at −100 mV (*4*). (*B*) Families of currents in control (*left*), 10 μM Zn^{2+} (*middle*) and after Zn^{2+} washout (*right*). Dotted line shows level of zero current. (*C*) Steady state P_o–V curves of the fast gate. ○, ■, and □ are control, in 10 μM Zn^{2+}, and wash, respectively (n = 4). Solid curves were drawn according to a simple voltage equilibrium: $P_o = P_{min} + (P_{max} - P_{min})/[1 + \exp(-zF(V - V_o)/RT)]$, with z = 0.7–0.83, P_{max} = 0.98–0.99, P_{min} = 0.01–0.16, and V_o = −73 to −85 mV. The differences among the three P_o-V curves were observed only at voltages more negative than −120 mV where the leak current contributed a relatively big fraction to the observed current. (*D*) Time constants of deactivation phase in period 3 plotted against membrane voltages. Symbols are as those in *C*.

these deactivation time constants is also minimal. The time constants in the presence and absence of Zn^{2+}, again, overlap with each other, particularly in the voltage range from −100 to −60 mV. In contrast, the reduction of the current by Zn^{2+} is observed at all membrane potentials (Fig. 2 *B*). Thus, the potent inhibition by Zn^{2+} shown in Fig. 1 is not likely due to an effect on the fast gating of the channel.

Apparent On and Off Rates of Zn^{2+} Inhibition Are Temperature Dependent

To further explore the mechanism of the Zn^{2+} effect, the kinetics of the inhibition was studied at a holding potential of −30 mV. As shown in Fig. 3 *A*, the amplitude of the whole oocyte current spontaneously decreases due to the closing of the slow gate, with the time to reach a steady state depending on the temperature. After the relaxation was close to a steady state, 10 μM Zn^{2+} was perfused in and out of the bath solution. The apparent on and off rates of Zn^{2+} inhibition were surprisingly slow. In addition, both rates were highly temperature dependent. To rule out the possibility that the slow kinetics and the temperature dependence of the Zn^{2+} effect were due to slow solution exchange, this exchange rate was measured using TEA to inhibit a *Shaker* K^+ channel with the inactivation ball removed (Fig. 3 *B*). Since TEA is known to block the *Shaker* K^+ channel with on and off rates in the micro- to millisecond time range (Hille, 1992), the time constants (∼1–3 s) measured from the TEA inhibition mostly reflect the delay of the solution exchange. Fig. 3 *C* compares the time constants of the Zn^{2+} inhibition of ClC-0 with those of the TEA inhibition of the *Shaker* K^+ channel. The apparent on and off rates of the Zn^{2+} inhibition of ClC-0 are clearly temperature dependent, whereas the solution exchange rate is not. Furthermore, the kinetics of the Zn^{2+} inhibition is much slower than that of the TEA inhibition. Except for high temperature conditions that gave relatively fast inhibitory kinetics, the rate of the solution exchange was usually 10-fold faster than that of the Zn^{2+} inhibition, indicating that the slow kinetics of the Zn^{2+} inhibition on ClC-0 do not arise from the solution exchange.

Extracellular Zn^{2+} Facilitates the Inactivation Relaxation

The strong temperature dependence of the inhibition kinetics suggests that a complicated process may be involved in Zn^{2+}-induced inhibition. With the inhibition showing such slow kinetics and high temperature dependence, it seems unlikely that Zn^{2+} acts as an open channel blocker to reduce the single-channel conductance of ClC-0. On the other hand, Zn^{2+} is more likely

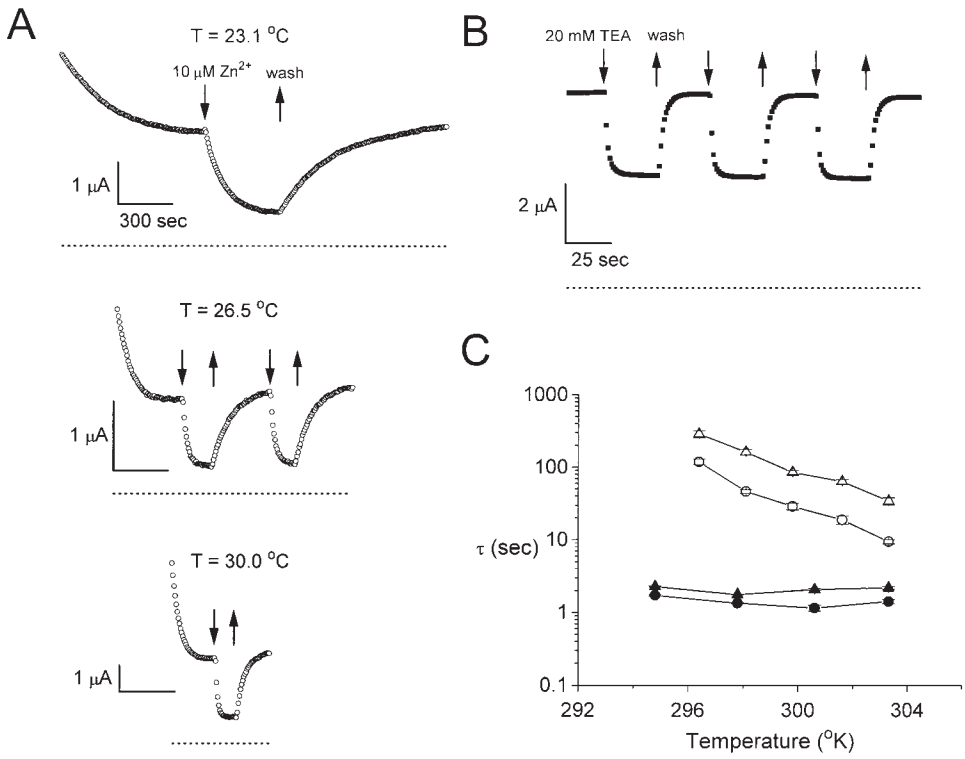

FIGURE 3. Kinetics of Zn^{2+} inhibition and recovery are temperature sensitive. (*A*) Inhibition of ClC-0 by 10 μM Zn^{2+} at three different temperatures. (*B*) Inhibition of *Shaker* K^+ channels by 20 mM TEA. The membrane potential was held at −80 mV and a 30-ms voltage pulse to +30 mV was given every second. Dotted lines in *A* and *B* represent zero-current level. (*C*) Comparison of the time constants of Zn^{2+} inhibition of ClC-0 (○ and △) with those of TEA inhibition of the *Shaker* K^+ channel (● and ▲). Circles, time constants of current inhibition; triangles, time constants of current recovery (n = 4–5).

to alter the slow gating of ClC-0, which intrinsically has a high Q_{10} (Pusch et al., 1997). To examine this possibility, the slow-gating relaxation of ClC-0 was studied at various temperatures with or without extracellular Zn^{2+} (Fig. 4). Consistent with a previous study (Pusch et al., 1997), the slow-gating relaxation follows a single-exponential decay. In the absence of Zn^{2+}, the time constant of the current relaxation is smaller with a higher temperature. At a fixed temperature, Zn^{2+} also speeds up the inactivation relaxation process; the relaxation time constant decreases with increasing Zn^{2+} concentration. From records like these, an Arrhenius plot of the time constants of the slow-gating relaxation at different Zn^{2+} concentrations was obtained (Fig. 5). The time constant, τ, depends on both temperature and Zn^{2+} concentration. In the absence of Zn^{2+}, the slope of the fit-

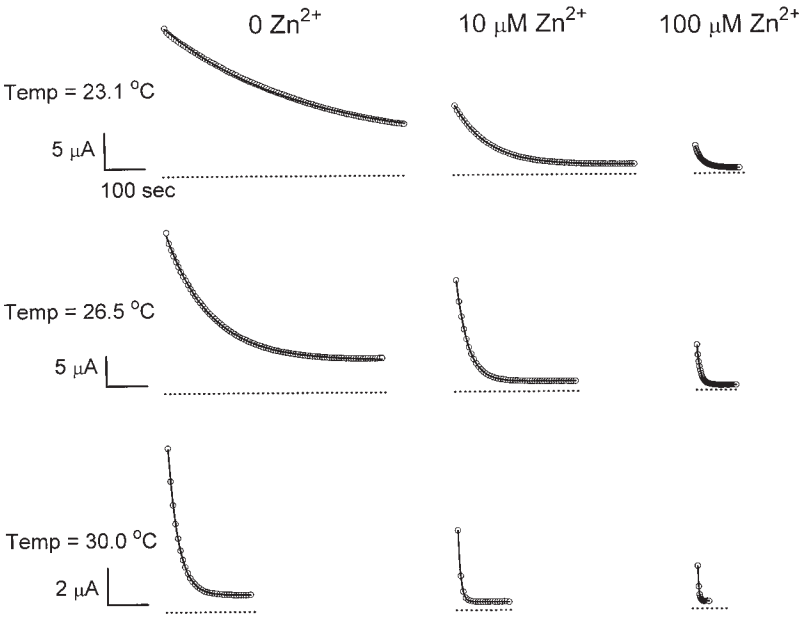

FIGURE 4. The slow-gating relaxation rate of ClC-0 is sensitive to both temperature and extracellular Zn^{2+}. Dotted lines show zero-current level. Solid curves were the best fit to single-exponential functions. Time constants at 0, 10, and 100 μM Zn^{2+} were: (23.1°C) 332.9, 81.2, and 17.6 s; (26.5°C) 109.3, 27.9, and 8.1 s; and (30.0°C) 25.4, 6.0, and 2.4 s, respectively.

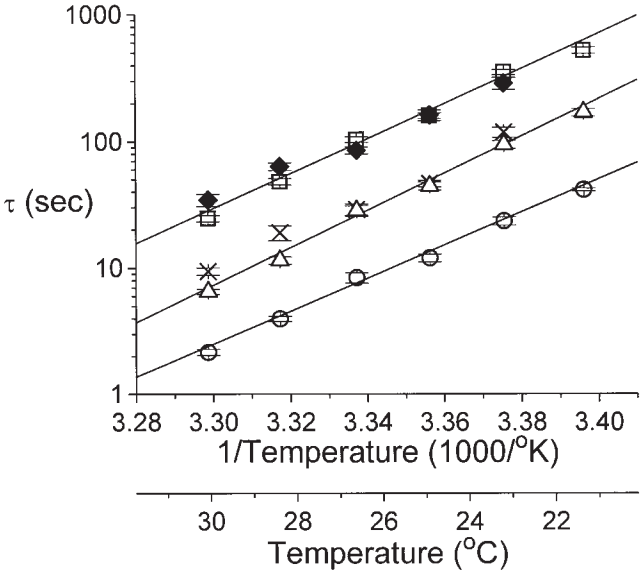

FIGURE 5. Arrhenius plot of the slow-gating relaxation time constants in various external $[Zn^{2+}]$. The time constant τ of the slow-gating relaxation was evaluated from experiments similar to those shown in Fig. 4 (n = 7–8). Solid lines were the best fit to $Y = A + BX$, where Y is $\log_{10}(\tau)$ and X is the inverse of temperature. External $[Zn^{2+}]$ (μM) and the Q_{10}s of the fitted lines were: (□) 0, 36.5; (△) 10, 46.2; (○) 100, 29.7. × and ◆ are the time constants of Zn^{2+} inhibition and recovery shown in Fig. 3 *C*.

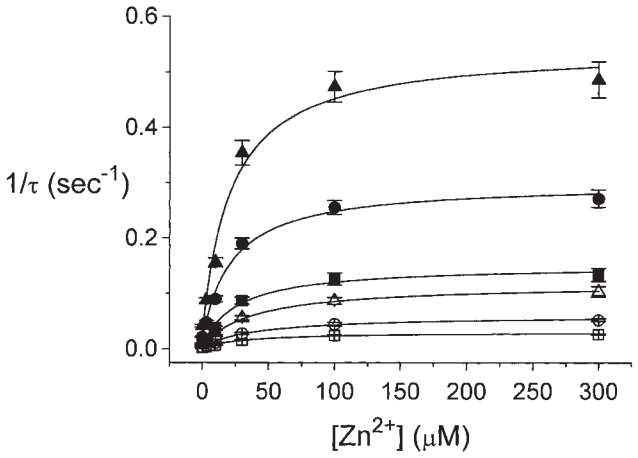

FIGURE 6. Slow-gating relaxation rate as a function of external $[Zn^{2+}]$. Data points were fitted to $Y = Y_o + X \cdot Y_\infty/(X + K_{1/2})$. The fitted $K_{1/2}$s (μM) and Y_∞/Y_o were: (21.3°C, □) 33.2, 29.2; (23.1°C, ○) 40.4, 35.9; (24.8°C, △) 39.0, 26.3; (26.5°C, ■) 26.6, 27.5; (28.3°C, ●) 22.0, 18.6; (30.0°C, ▲) 21.5, 18.7. The increase of the inactivation rate by Zn^{2+}, if all comes from the activation entropy, corresponds to an increase of ΔS of 24.3–29.8 J/mol per °K (see text for detailed discussion).

ted line gives a Q_{10} of ~37. Raising extracellular Zn^{2+} concentration shortens the relaxation time constant at all temperatures, but the slope of the fitted line does not change. When Zn^{2+} concentration is higher than 100 μM, the ability of Zn^{2+} to speed up the slow-gating kinetics appears to be saturated (Fig. 6). Curve fittings to hyperbolic equations give apparent half effective concentrations ($K_{1/2}$'s) from ~20–40 μM at various temperatures. The ratio between the rate at saturated Zn^{2+} (the fitted Y_∞) and in the absence of Zn^{2+} (the fitted Y_o) ranges from 18.6 to 35.9. As will be shown later, the $K_{1/2}$ and the ratio Y_∞/Y_o from this analysis are informative to assess the Zn^{2+}-binding affinities of the channel at different states.

A Four-State Scheme Describes the Inhibitory Effect of Zn^{2+}

The inhibition of ClC-0 by the extracellular Zn^{2+} shown above can be explained by a simple four-state model (Scheme I). Here, z represents Zn^{2+}, and O and I are the open and inactivated states of the channel. K_1 and K_2 are gating equilibrium constants between O and I and between Oz and Iz, whereas K_d and K_d* are apparent dissociation constants of Zn^{2+} binding to the open and inactivated channels, respectively. In this scheme, the closed state of the channel is ignored because most of the noninactivated channels are in the open state (versus close state) at a holding potential of −30 mV (Pusch et al. 1995; Chen and Miller, 1996). The binding and unbinding of Zn^{2+} to the channel are probably several orders of magnitude faster than the slow-gating transition because the latter operates at a time scale of tens to hundreds of seconds (Fig. 4). Thus, the rate-limiting steps of the steady state current inhibition by Zn^{2+} and the current recovery after Zn^{2+} washout must reside between Oz and Iz, and between O and I, respectively. This consideration predicts that the observed on rate of Zn^{2+} inhibition should be identical to the inactivation relaxation rate at the same Zn^{2+} concentration. Furthermore, the observed off rate of Zn^{2+} inhibition must also equal the inactivation relaxation rate in the absence of Zn^{2+}. Fig. 5 compares, at various temperatures, the apparent on and off rates of Zn^{2+} inhibition with the inactivation relaxation rates with or without 10 μM Zn^{2+}. Except for the comparisons of the on rate of Zn^{2+} inhibition with the inactivation rate at high temperatures, the above two predictions are fulfilled. At the highest two temperatures, 28.3° and 30.0°C, the time constants of the inhibition by 10 μM Zn^{2+} were 19.0 ± 5.1 (n = 4) and 9.4 ± 1.4 (n = 5) s, respectively, whereas the inactivation relaxation time constants at the same Zn^{2+} concentration were 11.5 ± 2.1 (n = 8) and 6.5 ± 0.9 (n = 8) s. The difference between these two cases is ~3–8 s, a value comparable to the time for the solution exchange. The 3–8-s delay, however, is relatively small in comparison with slow-gating relaxation rates in other experimental conditions. Thus, these results show that the apparent on rate for Zn^{2+} to inhibit the steady state current is indeed equal to the inactiva-

tion relaxation rate at the same Zn^{2+} concentration, indicating that Zn^{2+} is very likely acting on the inactivation process of the channel.

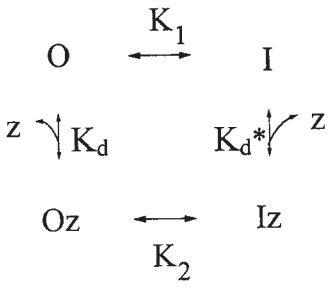

(SCHEME I)

The four-state scheme given above requires that the Zn^{2+} binding affinity of the inactivated channel be higher than that of the open channel; that is, $K_d > K_d^*$. This is because the ratio K_d/K_d^* must equal K_2/K_1, which is >1. Let transition rates α_1 and β_1 be the forward rate (the rate of inactivation) and the backward rate (the rate of recovery from inactivation) of the slow gating of the unliganded ClC-0, respectively, and α_2 and β_2 be those of the Zn^{2+}-bound channel. It can be shown that if Zn^{2+} increases only the forward rate (that is, $\beta_1 = \beta_2$), the $K_{1/2}$ obtained from Fig. 6 would be K_d. On the other hand, if the effect of Zn^{2+} is solely on β (that is, $\alpha_1 = \alpha_2$), $K_{1/2}$ would be K_d^*. The latter possibility can be ruled out even at this stage since the increase of β alone by Zn^{2+} would have led to a potentiation instead of an inhibition of the steady state current. There is, however, a possibility that Zn^{2+} may affect both the forward and backward rates of the slow-gating process. To address this question, it will be informative to evaluate the equilibrium between O and I by constructing the activation curve of the slow gate.

Effect of Zn^{2+} on the Activation Curve of the Slow Gate

The voltage-dependent activation of the slow gate was examined with a protocol shown on top of Fig. 7 *A*, in which a 7-s prepulse from 0 to −140 or −150 mV in −10-mV steps was followed by a 0.8-s test pulse at +40 mV. This voltage protocol had been used previously to examine the activation curve of the slow-gating process, and it was found that the 7-s prepulse is long enough to maximally activate the slow gate (Pusch et al., 1997). As shown in Fig. 7 *A*, Zn^{2+} inhibits the activation of the slow gate in a dose-dependent manner. Fig. 7 *B* plots the current measured at the test pulse as a function of the prepulse voltage. This quasi–steady state activation curve shows a biphasic response for the open probability of the slow gate. The peak of the activation curves is around −120 mV in this experiment carried out at 23.8°C. The activation curves at 19.8° and 28.0°C reveal a similar pattern of voltage dependence (Fig. 7 *C*). In all three temperatures, 10 and 100 μM Zn^{2+} do not change the biphasic behavior of the activation curve, suggesting that Zn^{2+} has little effect on the current-decreasing phase at very negative potentials. The nonmonotonic behavior of the activation curve has been observed previously (Ludewig et al., 1997; Fong et al., 1998). The current reduction at the hyperpolarized end of the curve may be due to an additional unknown mechanism that closes the channel with strong negative potential. Therefore, I have restricted my attention to the voltage range more depolarized than −120 mV to simplify the analysis. In all situations, Zn^{2+} inhibits currents at all voltages with approximately the same degree, suggesting that the inhibition has little voltage dependence. The fractional inhibition ranges from ~50 to 70% at 10 μM Zn^{2+} and ~80 to 95% at 100 μM Zn^{2+}.

Effect of Zn^{2+} Is Mostly on the Forward Rate of Inactivation

With information from kinetics as well as quasi–steady state equilibrium, it is possible to evaluate the rate constants of the slow-gating process. In the quasi–steady state activation curve, the current does not further decrease when the membrane potential is more depolarized than −30 mV (Fig. 7, *B* and *C*; also see Pusch et al., 1997). The noninactivated current fraction, obtained by normalizing the current amplitude at −30 mV (I) to the maximal current in the activation curve (I_{max}), can be expressed as a function of the forward (α) and backward (β) rate constants of the slow-gating process:

$$I/I_{max} = \beta/(\alpha+\beta). \quad (1)$$

In addition, the observed time constant τ of the slow-gating relaxation shown in Fig. 4 is also a function of α and β, with the following relation:

$$\tau = 1/(\alpha+\beta). \quad (2)$$

Table I lists, at three temperatures, the relaxation time constant τ and the steady state fraction of the noninactivated current, I/I_{max}. The calculated forward rate constant α and backward rate constant β are also shown. Without considering the leak current (numbers outside parentheses in Table I), both α and β increase with Zn^{2+}. The ratio between β at 100 μM Zn^{2+} (β_{100}) and in the absence of Zn^{2+} (β_0) ranges from ~2 to 5, whereas the ratio between α at 100 μM Zn^{2+} (α_{100}) and α in the absence of Zn^{2+} (α_0) ranges from ~13 to 18. Even under such situations where the analysis is contaminated with the leak current, most of the Zn^{2+} effect is on the forward rate α. When 1, 2, or 3% of the total current is considered as the leak, the ratio α_{100}/α_0 is not sensitive to variable leak fractions, whereas the ratio β_{100}/β_0 becomes ~2–4, 1–3, and 0.6–1.5, respectively. Clearly, as more of the current is subtracted, the effect of Zn^{2+} on β gets smaller. It is difficult to give an exact number for the leak fraction from these experi-

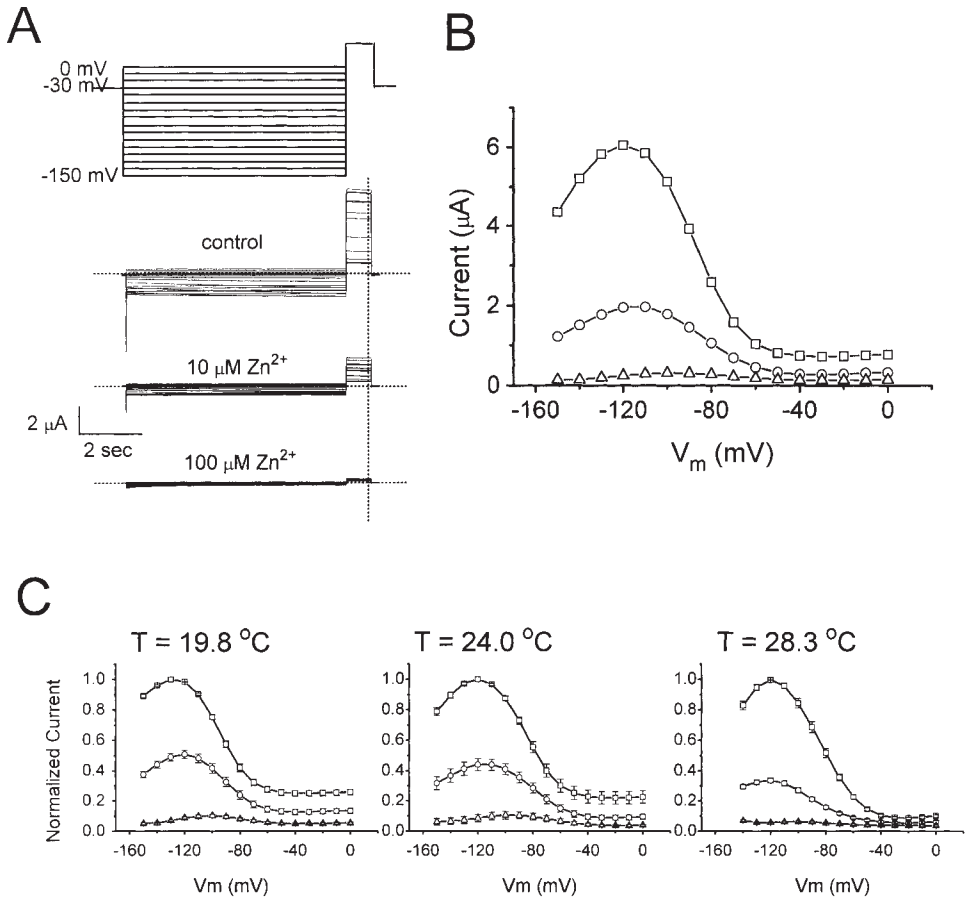

FIGURE 7. Effects of Zn^{2+} on the quasi–steady state activation curve of the slow gate. (*A*) Family of current traces elicited at 0, 10, and 100 μM Zn^{2+} with a voltage protocol shown on top. All traces were from the same oocyte at 24.0°C. The membrane potential was first held at −30 mV for the slow gating to reach steady state before each experiment started. Horizontal dotted lines indicate level of zero current. (*B*) Quasi–steady state activation curves at various Zn^{2+} concentrations from the experiment shown in *A*. The current amplitudes were measured at the vertical dotted line shown in *B*. □, ○, and △ represent control, 10, and 100 μM Zn^{2+}, respectively. (*C*) Averaged quasi–steady state activation curves at 19.8, 24.0, and 28.3°C. Symbols are as those in *B* (n = 3–5).

ments since ClC-0 does not close completely even at very large negative potentials (Chen and Miller, 1996; Ludewig et al., 1997). However, the leak currents observed from recordings of uninjected oocytes were usually ~0.1–0.2 μA at +40 mV, and the maximal currents of the oocytes for the experiments in Fig. 7 *C* were ~3–8 μA. Therefore, it seems reasonable to give a leak fraction of at least 2–3%. This number can also be independently checked by recording oocytes in 0 Cl^- solution (see MATERIALS AND METHODS).

The data corrected with leak subtraction are shown within parentheses in Table I. The leak fraction is cho-

TABLE I

Effects of Zn^{2+} on the Forward (α) and Backward (β) Rates of Inactivation

	τ (s)			I/I_{max}			β (× 10^{-3} s^{-1})				α (× 10^{-3} s^{-1})			
[Zn^{2+}] (μM)	0	10	100	0	10	100	β_0	β_{10}	β_{100}	β_{100}/β_0	α_0	α_{10}	α_{100}	α_{100}/α_0
19.8°C	1093.3	344.7	75.5	0.2508	0.1271	0.0516	0.229	0.369	0.683	2.98	0.686	2.532	12.562	18.31
				(0.2208)	(0.0971)	(0.0216)	(0.202)	(0.282)	(0.286)	1.42	(0.713)	(2.619)	(12.959)	18.18
24.0°C	235.4	67.1	17.8	0.2213	0.0891	0.0391	0.940	1.328	2.197	2.34	3.308	13.575	53.983	16.32
				(0.1913)	(0.0591)	(0.0091)	(0.813)	(0.881)	(0.511)	0.63	(3.435)	(14.022)	(55.669)	16.21
28.3°C	51.1	13.2	4.2	0.0908	0.0561	0.0378	1.777	4.250	9.000	5.06	17.792	71.508	229.095	12.88
				(0.0608)	(0.0261)	(0.0078)	(1.190)	(1.977)	(1.857)	1.56	(18.379)	(73.781)	(236.238)	12.85

The table lists the slow-gating relaxation time constant (τ) calculated from Fig. 5, the noninactivated current fraction (I/I_{max}) obtained from Fig. 7 *C*, the forward (α) and the backward (β) rates of inactivation at three different temperatures, and in 0, 10, and 100 μM Zn^{2+}. β was calculated by dividing I/I_{max} by τ (Eq. 1), whereas α was obtained by subtracting β from $1/\tau$ (Eq. 2). The numbers outside the parentheses were derived from original measured current without leak subtraction. The I/I_{max} values in parentheses were obtained by subtracting 0.03 from the original values outside parentheses and the α's and β's in parentheses were calculated accordingly.

sen to be 3% of the maximal current. Under this condition, the α's at 100 μM Zn^{2+} are ~13–18-fold larger than those in the absence of Zn^{2+}. On the other hand, Zn^{2+} has almost no effect on the backward rate β at all three temperatures. This argues that K_2/K_1 should be equal to α_2/α_1 if Scheme I is considered. The ratio Y_∞/Y_o from Fig. 6 can be used to approximate α_2/α_1 since β is small in comparison with α (compare β_0 and β_{100} with α_0 and α_{100} in Table I). The dissociation constant for Zn^{2+} binding to the open channel (K_d) is ~30 μM, whereas Y_∞/Y_o ranges from 18.6 to 35.9 (Fig. 6). To a first degree of approximation, the dissociation constant for Zn^{2+} binding to the inactivated channel (K_d*) should be ~1 μM. It is interesting to point out that K_d* should be close to the apparent $K_{1/2}$ of Zn^{2+} inhibition on the steady state current at −30 mV, where the O ↔ I transition favors the I state. Furthermore, the more the I state is favored (that is, the higher the K_1 value as the temperature is raised), the closer the observed affinity to K_d*. In Fig. 3 *A*, the fractional inhibition of the steady state current by 10 μM Zn^{2+} is >50%, consistent with the K_d* value inferred from the above analysis. The dose-dependent inhibition of the steady state current by Zn^{2+} performed at temperatures around 25–30°C usually gave an apparent $K_{1/2}$ of ~1–3 μM (Fig. 1 *B*).

DISCUSSION

Transition metal ions have long been used to explore the structure and function of ion channels. In the present study, I have shown that Zn^{2+} can reversibly inhibit ClC-0. The effect of Zn^{2+} on the fast gate is only minimal and cannot explain the magnitude of Zn^{2+} inhibition. Rather, Zn^{2+} appears to inhibit the channel by facilitating the slow-gating process. Such a coupled equilibrium system, in which the binding of a divalent metal ion is coupled to the inactivation of an ion channel, has been characterized on the *Shaker* K^+ channel (Yellen et al., 1994). The binding of Cd^{2+} to the external mouth of the *Shaker* channel via an engineered cysteine was found to modulate the C-type inactivation of the channel, with the Cd^{2+} affinity increased by 45,000-fold for the inactivated channel. This effect is due to a destabilization of the open state as well as a stabilization of the inactivated state of the *Shaker* channel. In the present study, although the Zn^{2+} affinity of the inactivated ClC-0 is only 30-fold higher than that of the open channel, the same principle of coupled binding still applies. The effect of Zn^{2+} on the slow-gating equilibrium of ClC-0 appears to come mostly from an increase of the forward rate constant of the inactivation.

The inhibition of ClC channels by transition metal ions was also found in ClC-1 and ClC-2. However, the apparent affinity of Zn^{2+} inhibition of ClC-0 is very different from those of ClC-1 and ClC-2. For the *Torpedo* channel, the apparent $K_{1/2}$ for Zn^{2+} to inhibit the steady state current is ~1–3 μM (Fig. 1 *B*). In contrast, Zn^{2+} and Cd^{2+} inhibit ClC-1 and ClC-2 with apparent $K_{1/2}$'s at least 50–100-fold higher (Kürz et al., 1997; Rychkov et al., 1997; Clark et al., 1998), suggesting a different inhibition mechanism. As the inhibition of ClC-0 by Zn^{2+} is through the facilitation of the slow gating, the lack of a high-affinity block in ClC-1 and ClC-2 by Zn^{2+} or Cd^{2+} may suggest the absence of a similar Zn^{2+}-sensitive, highly temperature-dependent slow-gating process in these two mammalian channels.

Although the four-state scheme (Scheme I) appears to explain well the effect of Zn^{2+} at a constant holding potential of −30 mV, problems with this simple scheme are obvious when the membrane potential is changed. In Scheme I, the same voltage and temperature dependence are assigned at the transitions O ↔ I and Oz ↔ Iz. Under this condition, hyperpolarization, which opens the slow gate and shifts the channel (Zn^{2+} bound or unbound) mostly to the O state, would reduce the Zn^{2+} inhibition since the Zn^{2+}-bound O state is conducting. At an extremely negative membrane potential, the current should be the same whether in the absence or presence of Zn^{2+}. In other words, Zn^{2+} must shift the activation curve to the left along the voltage axis without changing the maximal and minimal current levels (see modeling in Fig. 8 *A*). The experimental results in Fig. 7, however, show that this appears not to be the case.

The problem of Scheme I discussed above comes from naively assigning the slow gating as a simple process between only two states, O and I. Pusch et al. (1997) pointed out that any Markov-type model to describe the slow gating itself requires at least four states. Based on the quasi–steady state activation curves at different temperatures, they suggested the model shown in Scheme II. Here, O_1 and O_2 represent the two states in which the slow gate is open (that is, the noninactivated states), whereas I_1 and I_2 are the two states in which the slow gate is closed (the inactivated states). K_{AB}s are equilibrium constants between states A and B. The peculiar feature of this model is that the transitions between O and I ($O_1 \leftrightarrow I_1$ and $O_2 \leftrightarrow I_2$) are temperature, but not voltage, dependent. The voltage dependence instead resides in the transitions between states 1 and 2 ($O_1 \leftrightarrow O_2$ and $I_1 \leftrightarrow I_2$; Pusch et al., 1997). Thus, as long as the free energy of the slow-gating transition of channel population 1 differs from that of channel population 2 (that is, $K_{O1I1} \neq K_{O2I2}$), the open probability of the slow gate would reveal voltage dependence. At a fixed voltage (e.g., −30 mV), the total free energy of the slow-gating transition for all channels is constant at the same temperature, so Scheme II would automati-

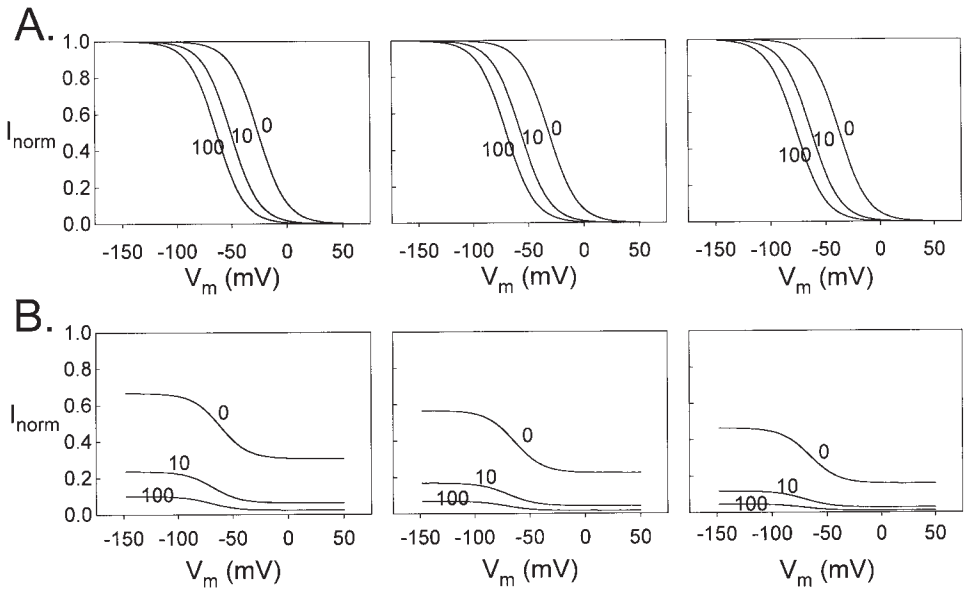

FIGURE 8. Simulation for the effect of Zn^{2+} on the quasi–steady state activation curve of the slow gate. Activation curves were generated based on Scheme I (*A*) and Scheme III (*B*) in the presence of 0, 10, and 100 μM Zn^{2+} at 20° (*left*), 24° (*middle*), and 28°C (*right*). The ratio of the occupation probability of any two states, *A* and *B*, is assumed to be of the form: $1/K_{AB} = P_A/P_B = \exp(-\Delta G_{AB}/RT) = \exp(\Delta S_{AB}/R - \Delta H_{AB}/RT + z_{AB}VF/RT)$, where K_{AB} is the equilibrium constant, and ΔG_{AB}, ΔS_{AB}, and ΔH_{AB} are the difference in Gibbs free energy, entropy, and enthalpy between the two states, respectively. *R*, *T*, and *F* have their usual meanings. V is the membrane voltage and z_{AB} is the "gating valence" describing the voltage dependence of the transition A ↔ B. The values of the above parameters in the absence of Zn^{2+} were the same as those in a previous paper (Pusch et al., 1997) except for ΔH_{O1O2}. They are shown as follows (ΔH in kJ/mol, ΔS in kJ/mol/°K): (*A*) $\Delta H_{OI} = -80$, $\Delta S_{OI} = -0.29$, $z_{OI} = -2$; (*B*) $\Delta H_{O1I1} = -77$, $\Delta S_{O1I1} = -0.26$, $z_{O1I1} = 0$, $\Delta H_{O1O2} = 10$, $\Delta S_{O1O2} = 0$, $z_{O1O2} = -2$, $\Delta H_{O2I2} = -78$, $\Delta S_{O2I2} = -0.27$, $z_{O2I2} = 0$. Assigning 10 kJ/mol for ΔH_{O1O2} makes all curves in *B* shift to the left by ~40 mV so that the curves from modeling are more similar to the experimental data with respect to their positions along the voltage axis. It does not affect the effect of Zn^{2+}, which shifts the curve from top to bottom. Even with this adjustment, the assigned values in *B* do not provide a superb prediction for the plateau at positive voltages as they give a much larger noninactivated fractional current than the data shown in Fig. 7. This difference is not important since the pattern of Zn^{2+} inhibition is basically the same as that in the experimental data. The numbers 0, 10, and 100 indicate Zn^{2+} concentrations.

cally reduce to a two-state process. Under such situations, Scheme I would be able to explain the effect of Zn^{2+} as being achieved from the analysis of the Zn^{2+} inhibition on the steady state current at −30 mV.

$$\begin{array}{ccc} & K_{O_1I_1} & \\ O_1 & \longleftrightarrow & I_1 \\ K_{O_1O_2} \updownarrow & & \updownarrow K_{I_1I_2} \\ O_2 & \longleftrightarrow & I_2 \\ & K_{O_2I_2} & \end{array}$$

(SCHEME II)

As Zn^{2+} apparently exerts its effect on the slow-gating process, one can examine whether Scheme II is valid by studying the effect of Zn^{2+} on the quasi–steady state activation curve. The examination can be illustrated in Scheme III. Here, the four states in front represent Scheme II and each of the four species is then connected to a Zn^{2+}-bound state. The dissociation constants for Zn^{2+} binding to the channels (K_d and K_d*) and the equilibrium gating constants among the Zn^{2+}-unbound states have the same meanings as those in Schemes I and II, respectively. To model the effects of Zn^{2+} on activation curves, the enthalpy and entropy of the transitions among Zn^{2+}-unbound states were taken from Pusch et al. (1997). In addition, two pieces of information from Fig. 6 are also used: the dissociation constant of Zn^{2+} binding to the open-state channel (K_d) is 30 μM, and the entropy difference of the slow-gating transition in the Zn^{2+}-bound channel is increased by 27 J/mol/°K. The latter is calculated from the ratio Y_∞/Y_o, according to transition state theory and assuming that the backward rate of the inactivation process is not affected by Zn^{2+} (see RESULTS). Fig. 8 *A* shows that Zn^{2+} shifts the activation curve along the voltage axis when only two states, O and I, are used to describe the slow gating (Scheme I). On the other hand, the activation curves derived from Scheme III show a Zn^{2+} inhibition pattern similar to the experimental results (Fig. 8 *B*). The curve shifts along the longitudinal axis by raising extracellular Zn^{2+}, a pattern similar to that made by increasing temperature (Pusch et al., 1997). This similarity is not surprising since a change in temperature is equivalent to a change in entropy with respect to their contributions to the free energy of the slow-gating process.

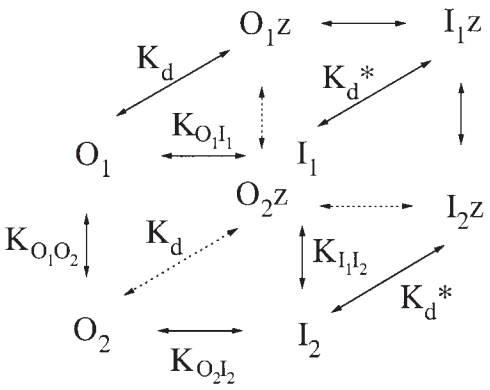

(SCHEME III)

Scheme III thus describes the effect of Zn^{2+} on the quasi–steady state activation curve well, but only at voltages more depolarized than −120 mV. As the membrane potential is more negative than −120 mV, the open probability of the slow gate becomes paradoxically smaller. There is very limited information about the slow gating at such hyperpolarized membrane potentials, so the underlying mechanism is difficult to address at the present time. However, the facilitation of inactivation upon depleting permeant ions has been observed in other channels (Baukrowitz and Yellen, 1995, 1996; Townsend and Horn, 1997). This possibility cannot be ruled out here since reduction of the intracellular Cl^- concentration, at least near the internal mouth of the channel, is very likely to occur in such a hyperpolarized condition. The slow gating of ClC-0 has long been known to couple to the Cl^- flux across the channel pore (Richard and Miller, 1990). Thus, the slow gating of ClC-0 could be more complicated than the above gating scheme if the Cl^- effect is considered.

The high activation energy of the inactivation of ClC-0 is consistent with a complex conformational change thought to involve subunit interaction between two protomers (Pusch et al., 1997). In the Arrhenius plot, Zn^{2+} simply shifts the line describing temperature dependence without altering the slope of the line (Fig. 5). This suggests that Zn^{2+} binding does not change the activation enthalpy of the slow-gating process, but results in a bigger entropy difference between the open and transition states. Assuming the transition state with or without Zn^{2+} has the same entropy, the open state must have a lower entropy in the presence than in the absence of Zn^{2+}. One can imagine that the complex slow-gating process may involve a step that requires some kind of order in the channel protein (or part of the channel protein, for example, a less movable loop), which renders the inactivation process relatively unfavorable. Zn^{2+}, in binding to the channel, may facilitate this process by providing the order that would otherwise be more difficult to reach in the absence of Zn^{2+}. This suggestion, however, is only one of the many interpretations based on thermodynamic arguments. The structural evidence to support this implication awaits more characterization of the channel molecule.

In summary, I have shown that Zn^{2+} can reversibly inhibit the ClC-0 Cl^- channel from *Torpedo* electroplax. This effect is likely due to an increase of the inactivation rate of the channel with little changes on the rate of recovery from the inactivation state. The molecular structure of the slow gate and how it functions are largely unknown. Zn^{2+}, due to its effect on the inactivation process of ClC-0, may be used to further explore the slow gating of ClC-0 in the future.

I thank Prof. Chris Miller, who initiated this project by showing that the ash of burned spider venom retained the ability to inhibit ClC-0 just as potently as the fresh venom. I would also like to thank Drs. Tzyh-Chang Hwang and Ru-Chi Shieh for their comments on the manuscript.

This research was supported in part by grants NSC86-2314-B010-123T and NSC87-2314-B010-103 from the National Science Council, and also by a grant DOH88-HR-813 from National Health Research Institutes, Taiwan, ROC.

Original version received 4 May 1998 and accepted version received 1 September 1998.

REFERENCES

Backx, P.H., D.T. Yue, J.H. Lawrence, E. Marban, and G.F. Tomaselli. 1992. Molecular localization of an ion-binding site within the pore of mammalian sodium channels. *Science.* 257:248–251.

Baukrowitz, T., and G. Yellen. 1995. Modulation of K^+ current by frequency and external $[K^+]$: a tale of two inactivation mechanisms. *Neuron.* 15:951–960.

Baukrowitz, T., and G. Yellen. 1996. Use-dependent blockers and exit rate of the last ion from the multi-ion pore of a K^+ channel. *Science.* 271:653–656.

Bretag, A.H., M.J. Fietz, and R.R.J. Bennet. 1984. The effects of zinc and other transition metal ions on rat skeletal muscle. *Proc. Aust. Physiol. Pharmacol. Soc.* 15:146P. (Abstr.)

Chen, T.-Y., and C. Miller. 1996. Nonequilibrium gating and voltage dependence of the ClC-0 Cl^- channel. *J. Gen. Physiol.* 108: 237–250.

Clark, S., S.-E. Jordt, T.J. Jentsch, and A. Mathie. 1998. Characterization of the hyperpolarization-activated chloride current in dissociated rat sympathetic neurons. *J. Physiol. (Lond.).* 506:665–678.

Fong, P., A. Rehfeldt, and T.J. Jentsch. 1998. Determination of slow gating in ClC-0, the voltage-gated chloride channel of *Torpedo*

marmorata. *Am. J. Physiol.* 274:C966–C973.

Gordon, S.E., and W.N. Zagotta. 1995. A histidine residue associated with the gate of the cyclic nucleotide-activated channels in rod photoreceptors. *Neuron*. 14:177–183.

Hanke, W., and C. Miller. 1983. Single chloride channels from *Torpedo* electroplax: activation by protons. *J. Gen. Physiol.* 82:25–45.

Hille, B. 1992. Mechanisms of block. *In* Ion Channels of Excitable Membranes. 2nd ed. B. Hille, editor. Sinauer Associates, Inc. Sunderland, MA. 390–422.

Hutter, O.F., and A.E. Warner. 1967. Action of some foreign cations and anions on the chloride permeability of frog muscle. *J. Physiol. (Lond.)*. 189:445–460.

Jentsch, T.J., K. Steinmeyer, and G. Schwarz. 1990. Primary structure of *Torpedo marmorata* chloride channel isolated by expression cloning in *Xenopus* oocytes. *Nature*. 348:510–514.

Karpen, J.W., R.L. Brown, L. Stryer, and D.A. Baylor. 1993. Interactions between divalent cations and the gating machinery of cyclic GMP-activated channels in salamander retinal rods. *J. Gen. Physiol.* 101:1–25.

Kürz, L.L., S. Wagner, A.L. George, Jr., and R. Rüdel. 1997. Probing the major skeletal muscle chloride channel with Zn^{2+} and other sulfhydryl-reactive compounds. *Pflügers Arch.* 433:357–363.

Liu, Y., M. Holmgren, M.E. Jurman, and G. Yellen. 1997. Gated access to the pore of a voltage-dependent K^+ channel. *Neuron*. 19: 175–184.

Ludewig, U., M. Pusch, and T.J. Jentsch. 1996. Two physically distinct pores in the dimeric ClC-0 chloride channel. *Nature*. 383: 340–343.

Ludewig, U., T.J. Jentsch, and M. Pusch. 1997. Analysis of a protein region involved in permeation and gating of the voltage-gated *Torpedo* chloride channel ClC-0. *J. Physiol. (Lond.)*. 498:691–702.

Middleton, R.E., D.J. Pheasant, and C. Miller. 1994. Purification, reconstitution, and subunit composition of a voltage-gated chloride channel from *Torpedo* electroplax. *Biochemistry*. 33:13189–13198.

Middleton, R.E., D.J. Pheasant, and C. Miller. 1996. Homodimeric architecture of a ClC-type chloride ion channel. *Nature*. 383: 337–340.

Miller, C. 1982. Open-state substructure of single chloride channels from *Torpedo* electroplax. *Philos. Trans. R. Soc. Lond. B Biol. Sci.* 299:401–411.

Miller, C., and E.A. Richard. 1990. The voltage-dependent chloride channel of *Torpedo* electroplax: intimations of molecular structure from quirks of single-channel function. *In* Chloride Transporters. A. Leefmans and J. Russell, editors. Plenum Publishing Corp., New York. 383–405.

Miller, C., and M.M. White. 1984. Dimeric structure of single chloride channels from *Torpedo* electroplax. *Proc. Natl. Acad. Sci. USA*. 81:2772–2775.

Pusch, M., and T.J. Jentsch. 1994. Molecular physiology of voltage-gated chloride channels. *Physiol. Rev.* 74:813–825.

Pusch, M., U. Ludewig, and T.J. Jentsch. 1997. Temperature dependence of fast and slow gating relaxations of ClC-0 chloride channels. *J. Gen. Physiol.* 109:105–116.

Pusch, M., U. Ludewig, A. Rehfeldt, and T.J. Jentsch. 1995. Gating of the voltage-dependent chloride channel ClC-0 by the permeant anion. *Nature*. 373:527–531.

Richard, E.A., and C. Miller. 1990. Steady-state coupling of ion-channel conformations to a transmembrane ion gradient. *Science*. 247:1208–1210.

Rychkov, G.Y., D.S. Astill, B. Bennetts, B.P. Hughes, A.H. Bretag, and M.L. Roberts. 1997. pH-dependent interactions of Cd^{2+} and a carboxylate blocker with the rat ClC-1 chloride channel and its R304E mutant in the sf-9 insect cell line. *J. Physiol. (Lond.)*. 498: 691–702.

Stanfield, P.R. 1970. The differential effects of tetraethylammonium and zinc ions on the resting conductance of frog skeletal muscle. *J. Physiol. (Lond.)*. 209:231–256.

Steinmeyer, K., C. Ortland, and T.J. Jentsch. 1991. Primary structure and functional expression of a developmentally regulated skeletal muscle chloride channel. *Nature*. 354:301–304.

Townsend, C., and R. Horn. 1997. Effect of alkali metal cations on slow inactivation of cardiac Na^+ channels. *J. Gen. Physiol.* 110:23–33.

White, M.M., and C. Miller. 1979. A voltage-gated anion channel from electric organ of *Torpedo californica*. *J. Biol. Chem.* 254: 10161–10166.

Yellen, G., D. Sodickson, T.-Y. Chen, and M.E. Jurman. 1994. An engineered cysteine in the external mouth of a K^+ channel allows inactivation to be modulated by metal binding. *Biophys. J.* 66:1068–1075.